Supplementary Information for

Upgrading of nitrate to hydrazine through cascading electrocatalytic ammonia production with controllable N-N coupling

Shunhan Jia[1,2], Libing Zhang[1,2], Hanle Liu[1,2,3], Ruhan Wang[1,2], Xiangyuan Jin[1,2], Limin Wu[1,2], Xinning Song[1,2], Xingxing Tan[1], Xiaodong Ma[1], Jiaqi Feng[1,4], Qinggong Zhu[1,2], Xinchen Kang[1,2], Qingli Qian[1,2], Xiaofu Sun[1,2,*], Buxing Han[1,2,5,*]

[1] Beijing National Laboratory for Molecular Sciences, CAS Laboratory of Colloid and Interface and Thermodynamics, CAS Research/Education Center for Excellence in Molecular Sciences, Center for Carbon Neutral Chemistry, Institute of Chemistry, Chinese Academy of Sciences, Beijing 100190, China

[2] School of Chemical Sciences, University of Chinese Academy of Sciences, Beijing 100049, China

[3] College of Chemistry, Nankai University, Tianjin 300071, China

[4] College of Chemical Engineering and Environment, China University of Petroleum, Beijing 102249, China

[5] Shanghai Key Laboratory of Green Chemistry and Chemical Processes, State Key Laboratory of Petroleum Molecular & Process Engineering, School of Chemistry and Molecular Engineering, East China Normal University, Shanghai 200062, China

*Email: sunxiaofu@iccas.ac.cn (X.F.S.); hanbx@iccas.ac.cn (B.X.H.)

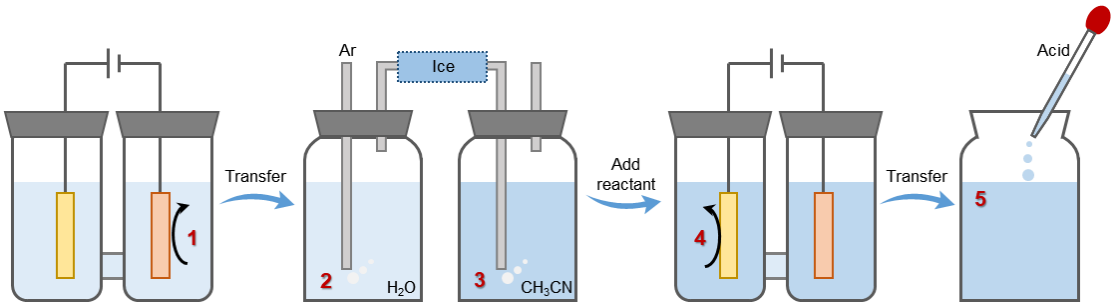

Figure S1. Illustration of reaction pathway of electrocatalytic upgrading of NO_x to N_2H_4 through the following steps: 1. Electroreduction of NO_x to NH_3; 2. Remove NH_3 with Ar; 3. Collected NH_3 in electrolyte; 4. Ketone-mediated N-N coupling; 5. Hydrolysis to obtain N_2H_4.

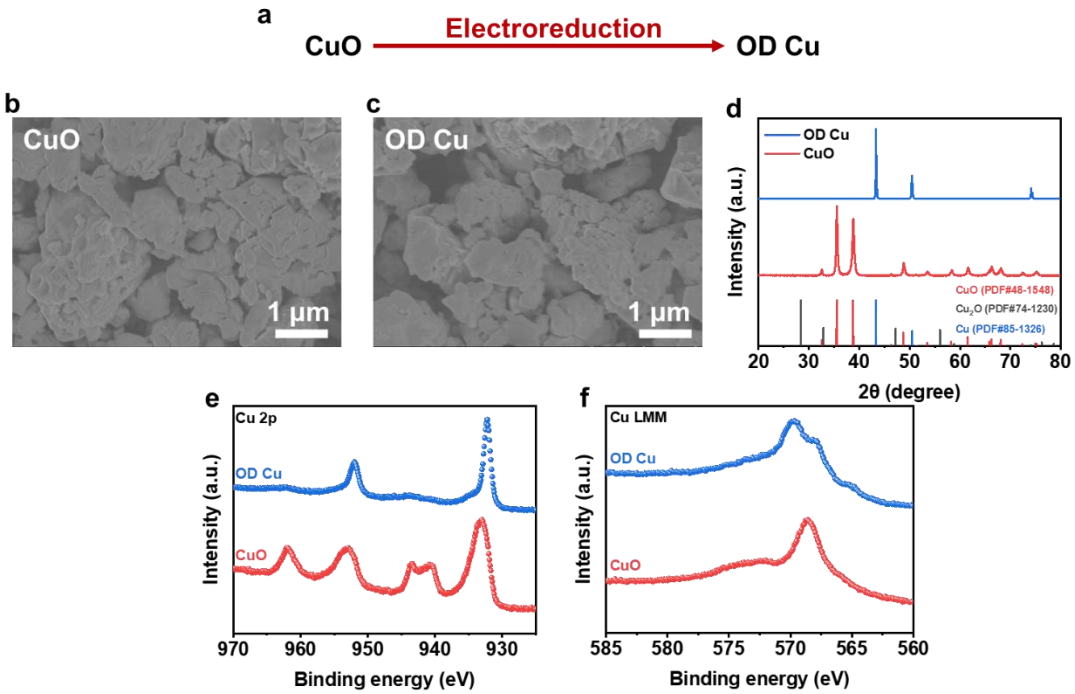

Figure S2. (a) Illustration of the generation of OD Cu catalyst. SEM image of (b) CuO and (c) OD Cu catalyst. (d) XRD patterns of CuO and OD Cu catalyst. (e) XPS spectra in the regions of Cu 2p and (f) Cu Auger LMM spectra of CuO and OD Cu catalyst.

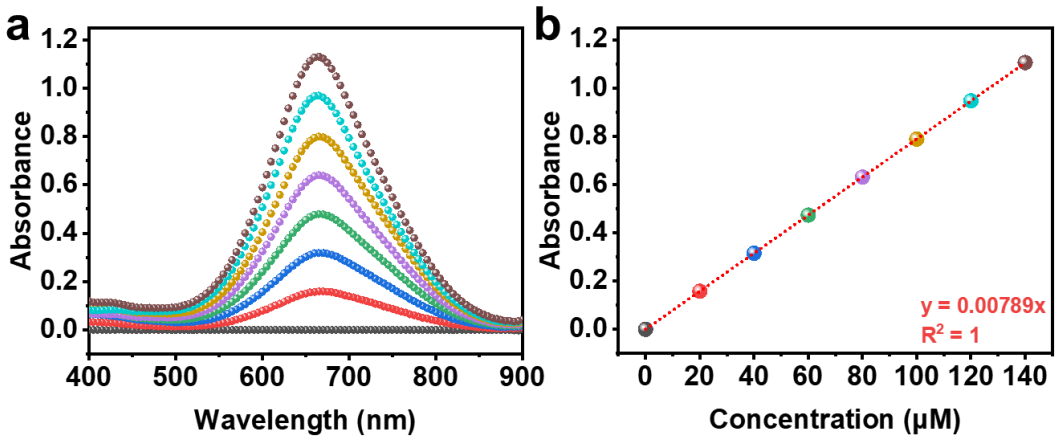

Figure S3. (a) UV-vis spectra of various concentration of NH_3. (b) The corresponding standard calibration curve for the assessment of NH_3.

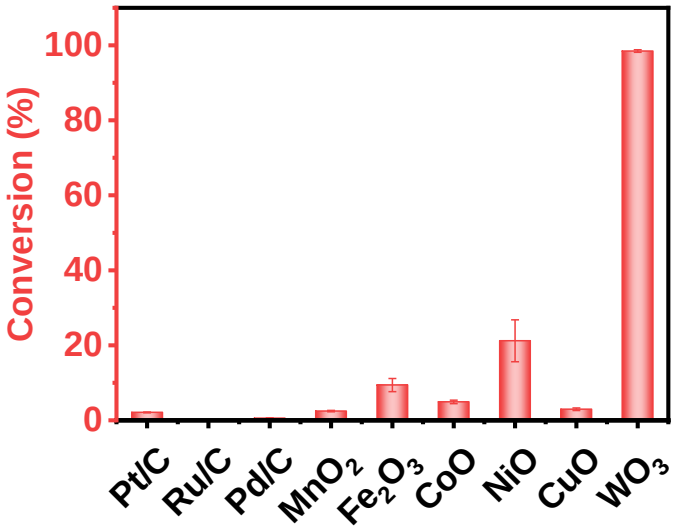

Figure S4. Catalyst screening for N_2H_4 synthesis by using different catalysts.

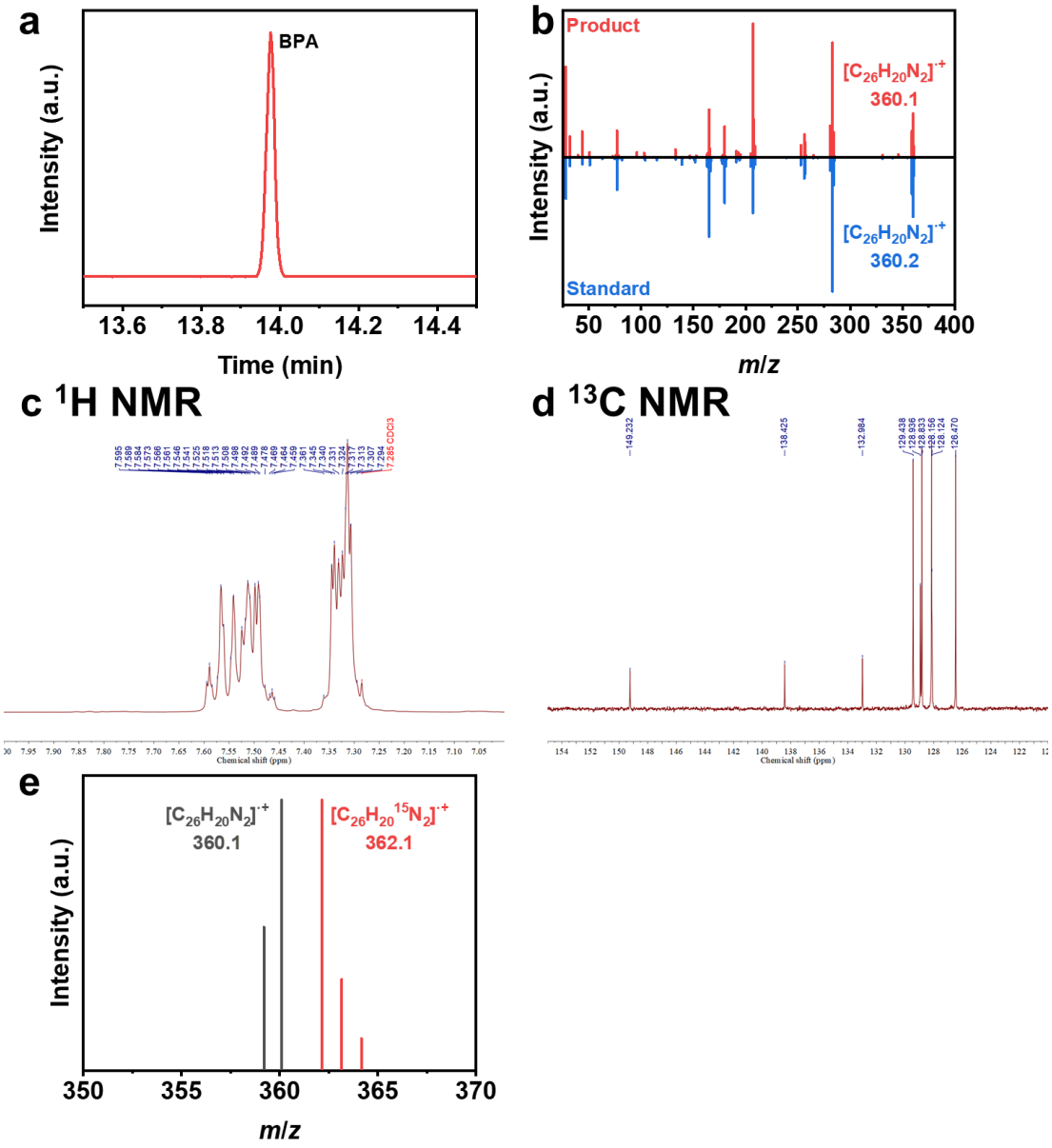

Figure S5. (a) GC and (b) MS spectrum of BPA. (c) ^{1}H NMR and (d) ^{13}C NMR spectrum of BPA. (e) MS of BPA generated from ^{15}N KNO_3.

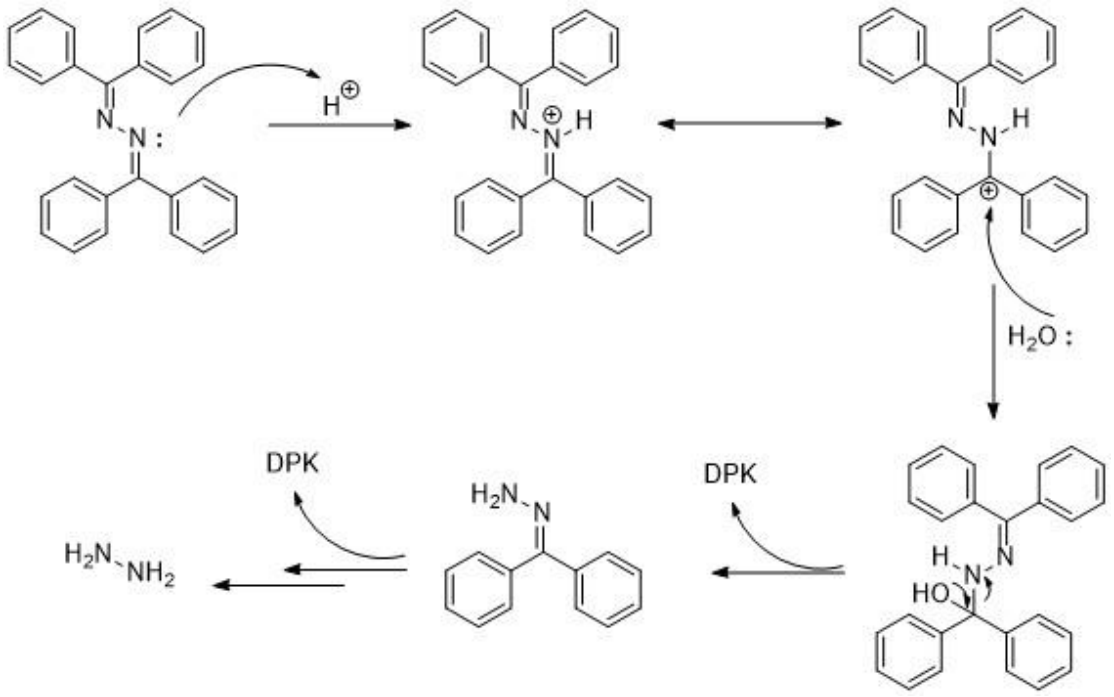

Figure S6. The mechanism of BPA hydrolysis in acid aqueous solution.

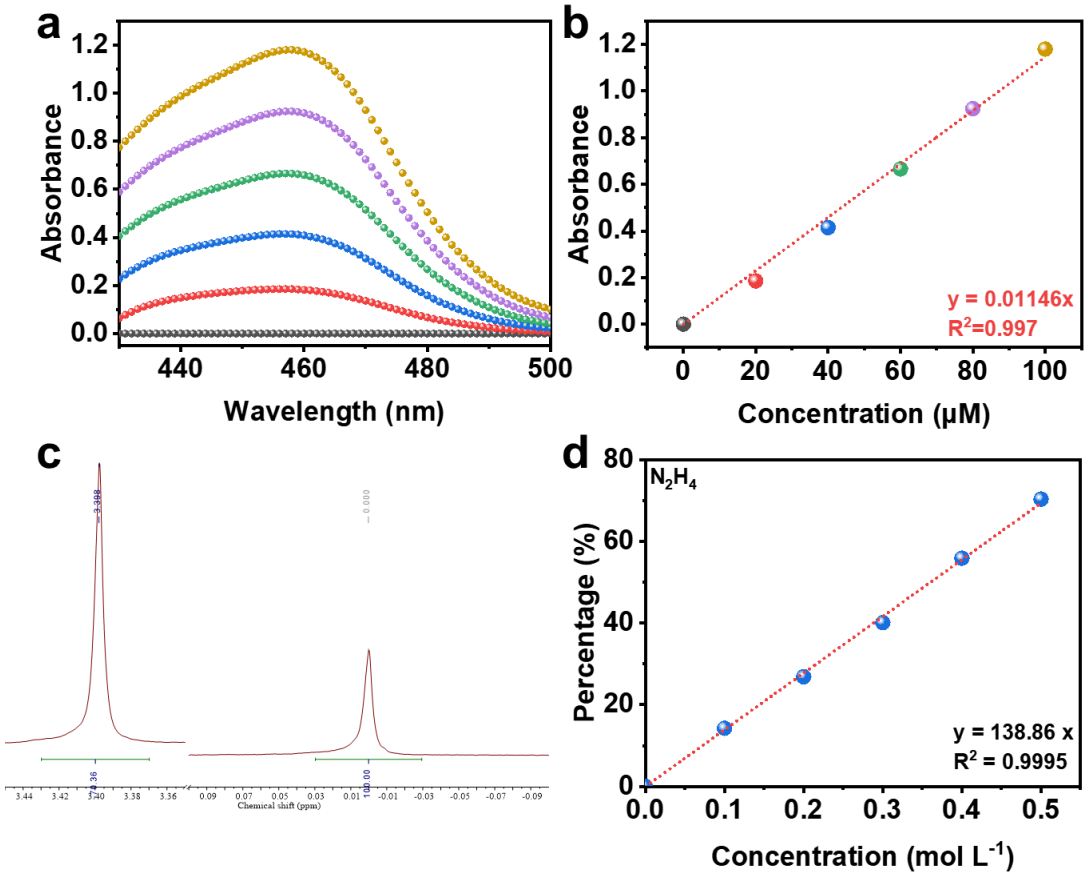

Figure S7. (a) UV-vis spectra of various concentration of N_2H_4. (b) The corresponding standard calibration curve for the assessment of N_2H_4 using UV-vis spectra. (c) ^1H NMR spectrum of 0.5 mol L^{-1} of N_2H_4 standard and DSS interior label. (d) The corresponding standard calibration curve for the assessment of N_2H_4 using ^1H NMR.

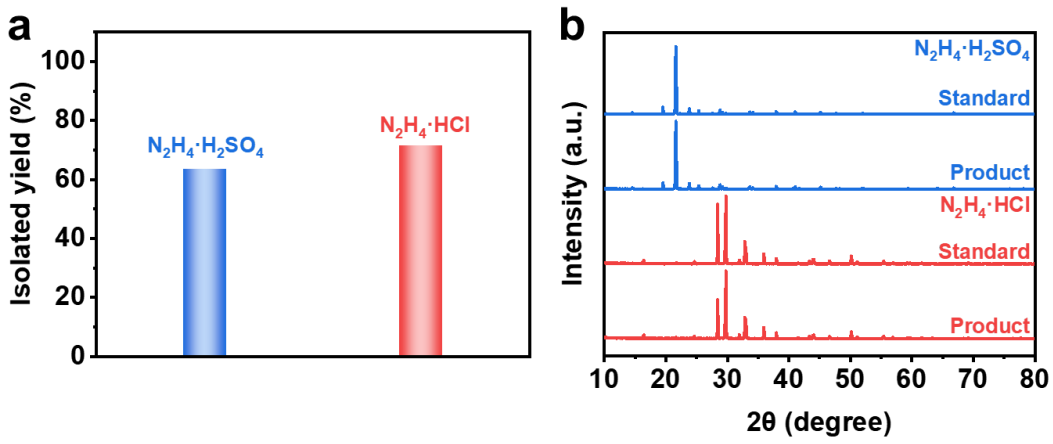

Figure S8. (a) Isolated yield and (b) corresponding XRD patterns of isolated N_2H_4 salts products compared with standard sample.

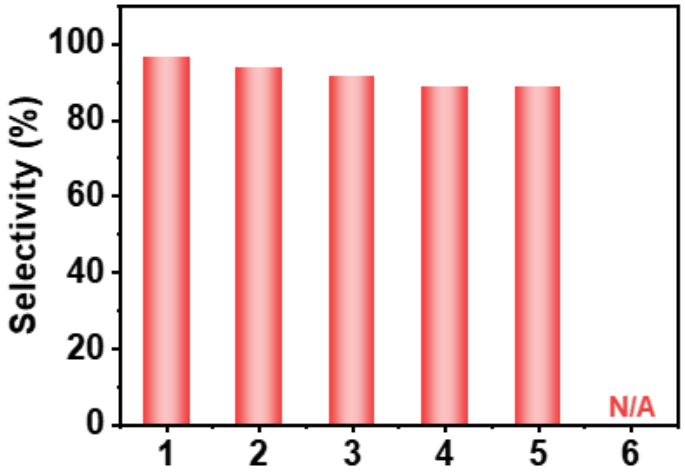

Figure S9. Selectivity of the nitrogenous species during the electrocatalytic upgrading of NO_x to N_2H_4 through several steps as following: 1. Electroreduction of NO_x to NH_3; 2. Remove NH_3 with Ar; 3. Collected NH_3 in electrolyte; 4. Ketone-mediated N-N coupling; 5. Hydrolysis to obtain N_2H_4; 6. Direct NH_3 oxidation to N_2H_4.

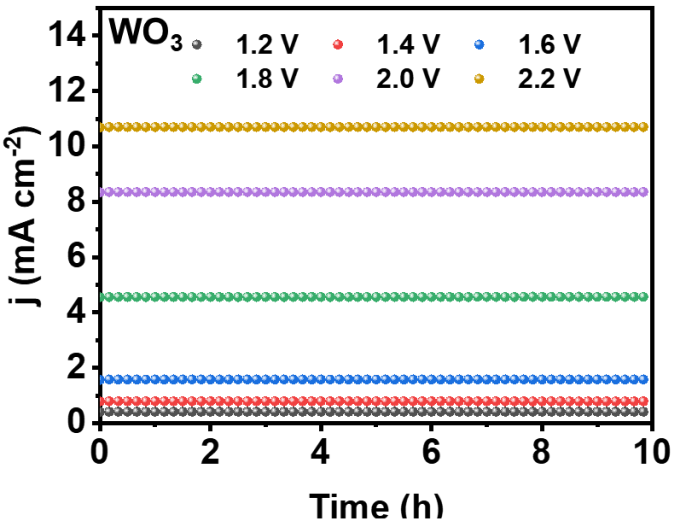

Figure S10. Chronoamperometry curves of BPA formation from 1.2 V to 2.2 V over WO_3 electrocatalyst.

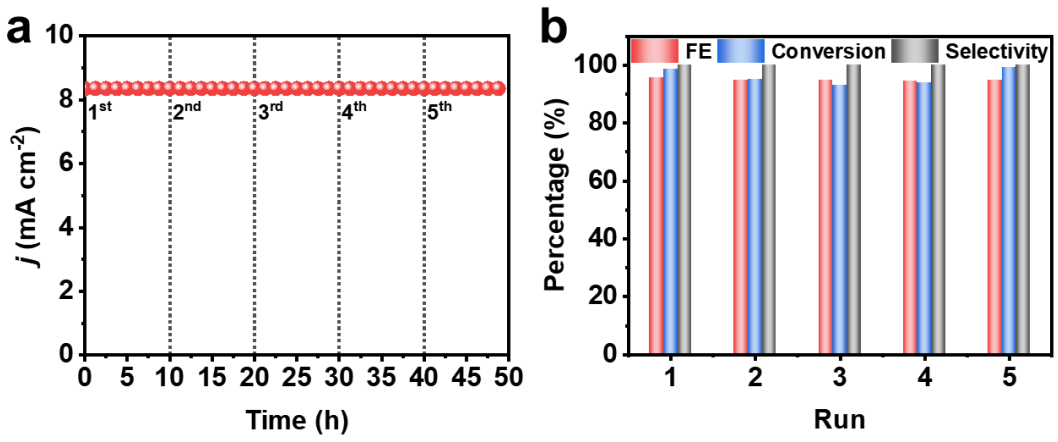

Figure S11. (a) Chronoamperometry curves and (b) BPA FE (red), NH_3 conversion (blue), and BPA selectivity (gray) of WO_3 during consecutive recycling tests at 2.0 V.

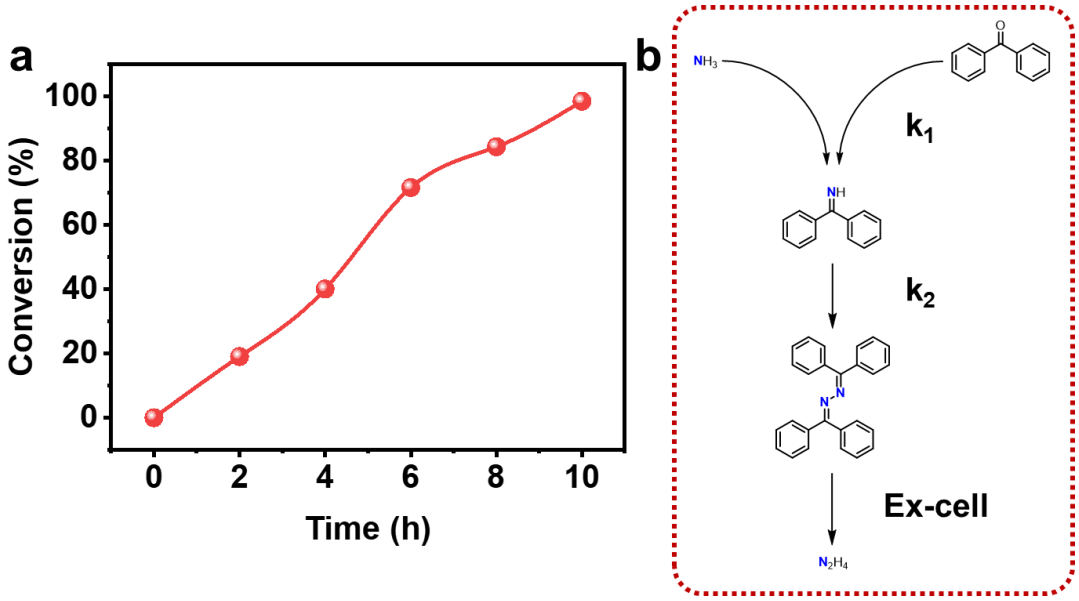

Figure S12. (a) Kinetic curve of time-dependance BPA formation on WO_3 under optimal conditions. (b) Reaction pathway of NH_3 to BPA.

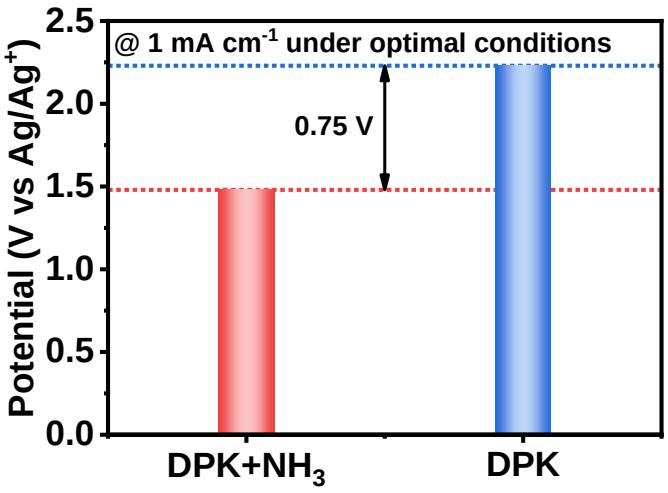

Figure S13. The potentials derived from LSV on WO_3 catalyst with DPK with and without NH_3 at a current density of 1 mA cm^{-2}.

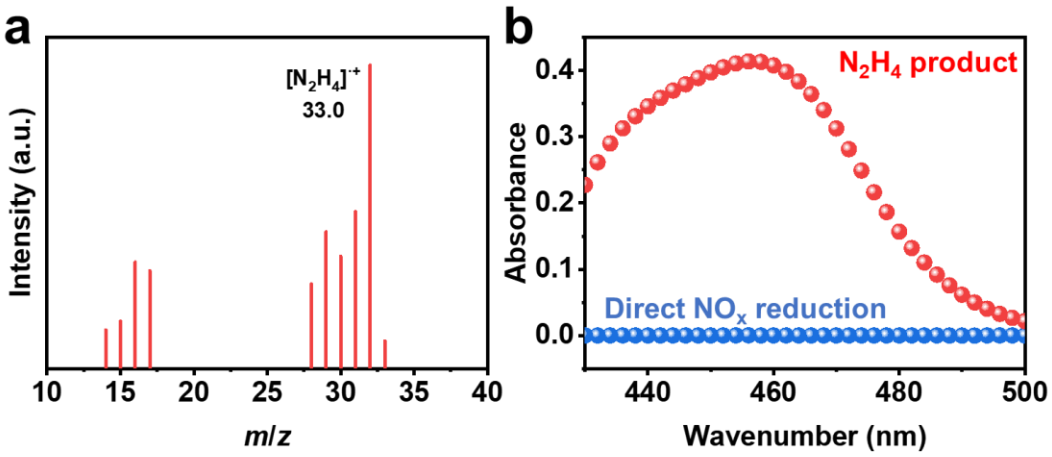

Figure S14. (a) MS of N2H4 product generated from BPA. (b). Comparison of the N_2H_4 products of N_2H_4 synthesis reported in this study and direct NO_x reduction through UV-vis spectrometry.

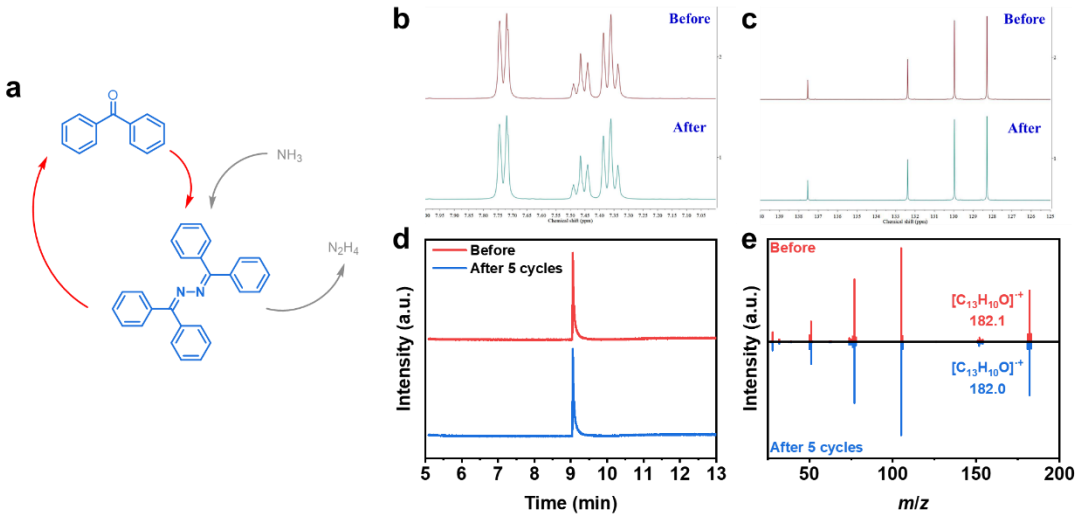

Figure S15. (a) illustration of the reusability of DPK. (b) ^{1}H NMR spectra, (c) ^{13}C NMR spectra, (d) GC curves, and (e) MS spectra of initial BPA mediator and regenerated BPA after five cycles.

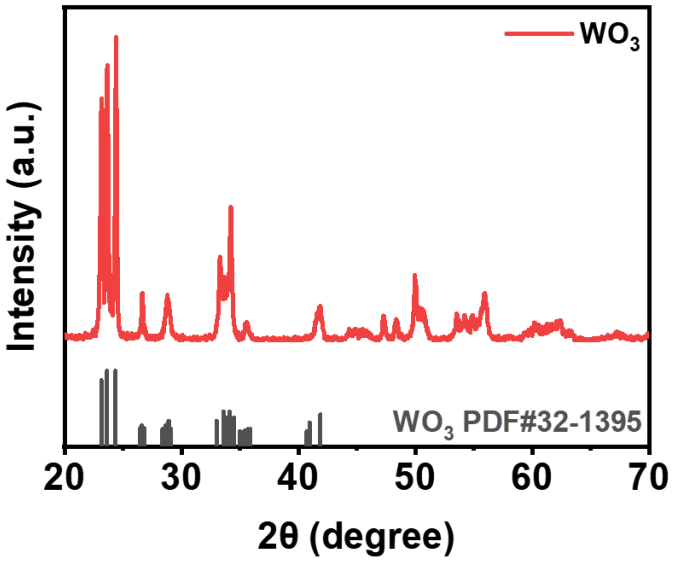

Figure S16. XRD patterns of WO_3 electrocatalyst.

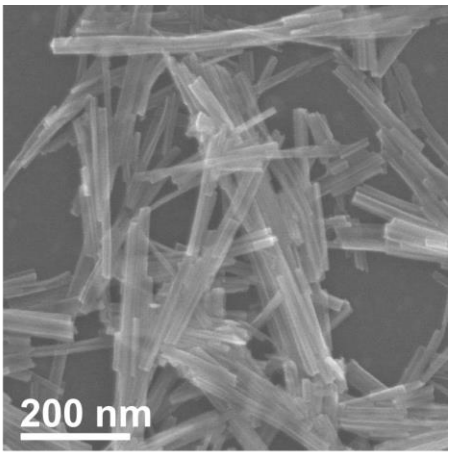

Figure S17. SEM image of WO_3 electrocatalyst.

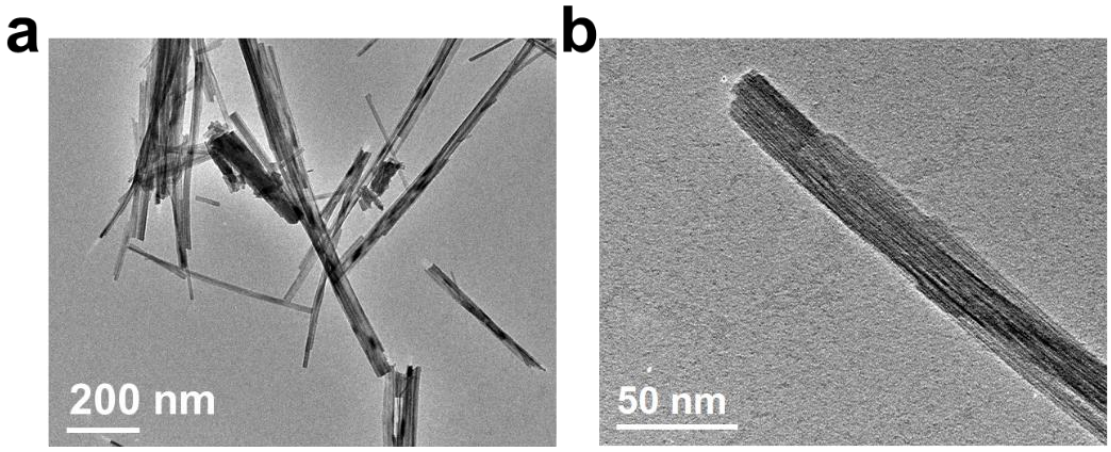

Figure S18. TEM image of WO_3 electrocatalyst at (a) low resolution and (b) high resolution.

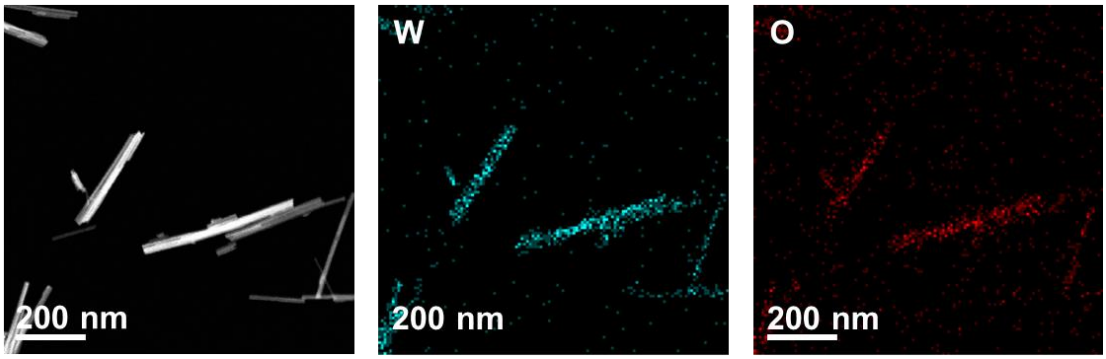

Figure S19. EDX mapping images of WO_3 electrocatalyst.

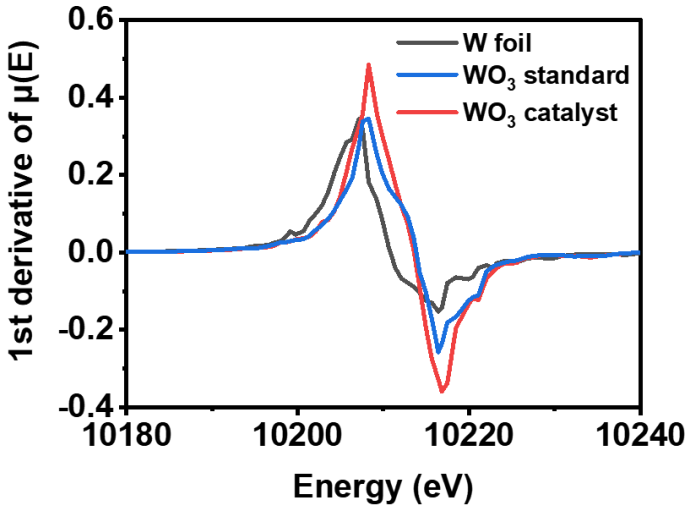

Figure S20. The first derivative of XANES spectra of W L_3-edge in WO_3 catalyst, WO_3 standard, and W foil.

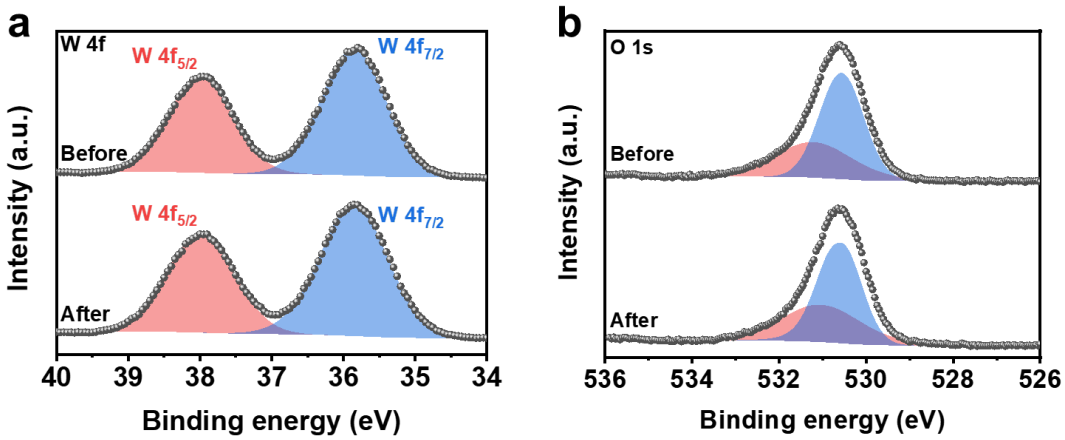

Figure S21. XPS spectra of WO_3 electrocatalyst in the regions of (a) W 4f and (b) O 1s.

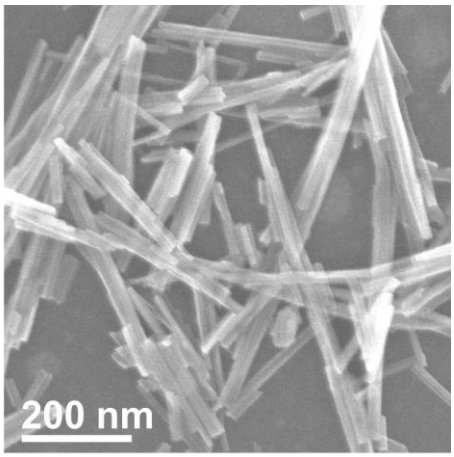

Figure S22. SEM image of WO_3 electrocatalyst after reusability test.

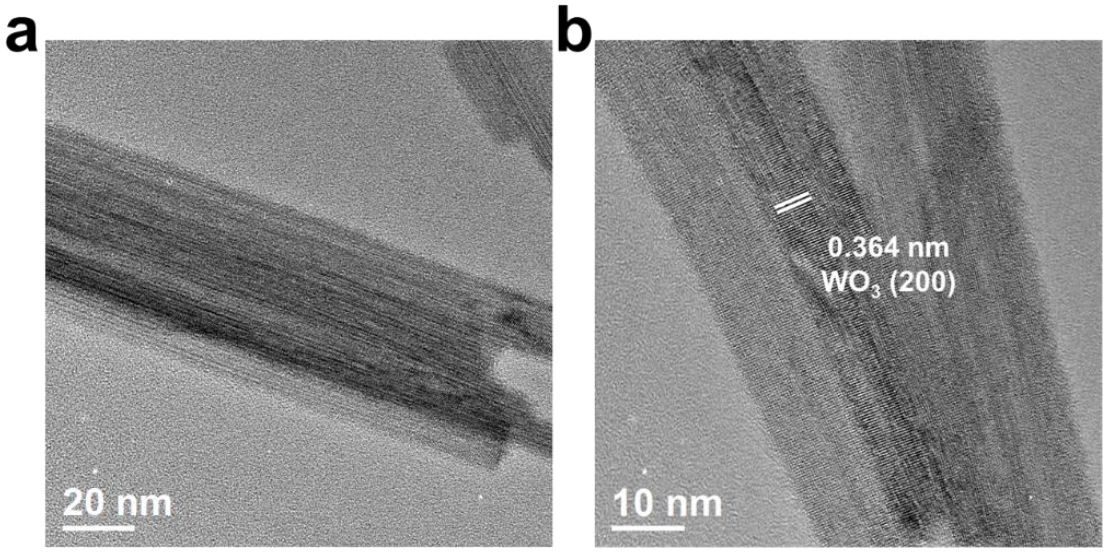

Figure S23. TEM image of WO_3 electrocatalyst after reusability test at (a) low resolution and (b) high resolution.

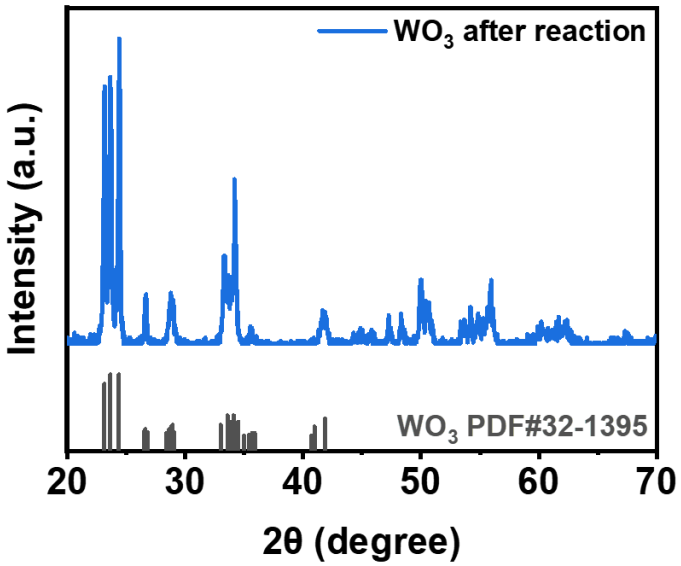

Figure S24. XRD pattern of WO_3 electrocatalyst after reusability test.

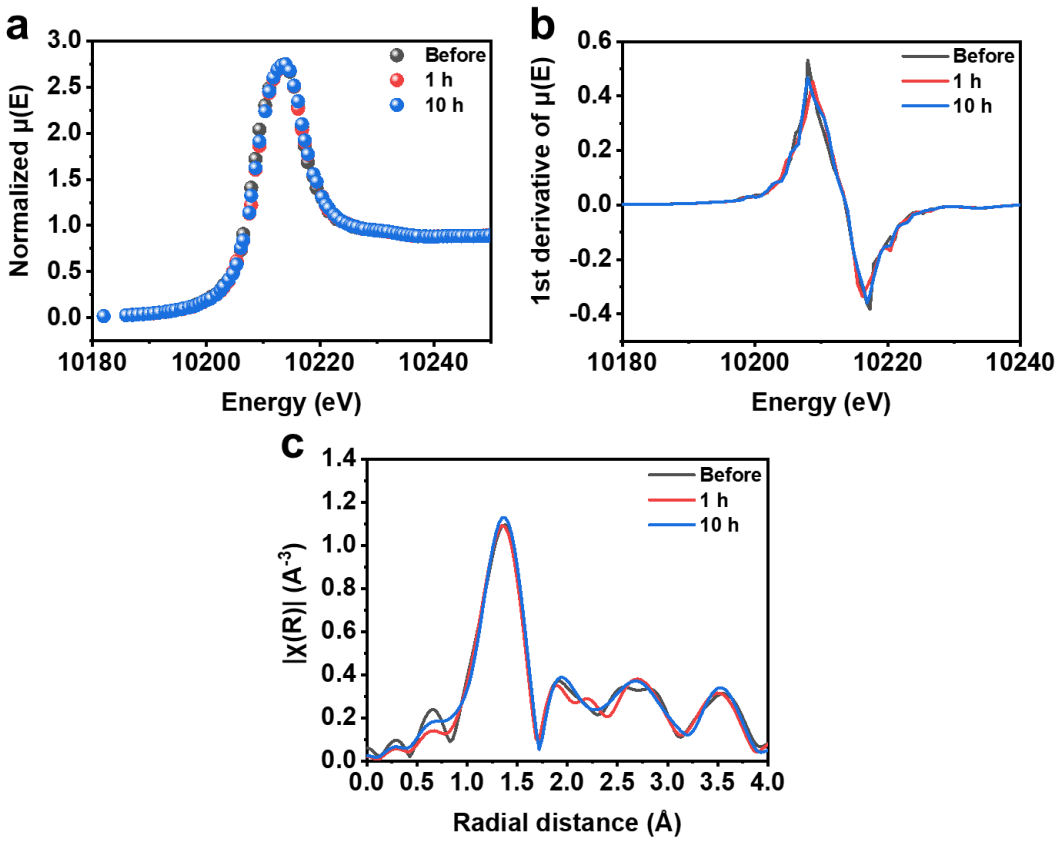

Figure S25. (a) XANES spectra, (b) the first derivative of XANES spectra of W L_3-edge, and (c) L_3-*edge* FT EXAFS spectra of the WO_3 catalyst after electrolysis for 0 h, 1 h, and 10h, respectively.

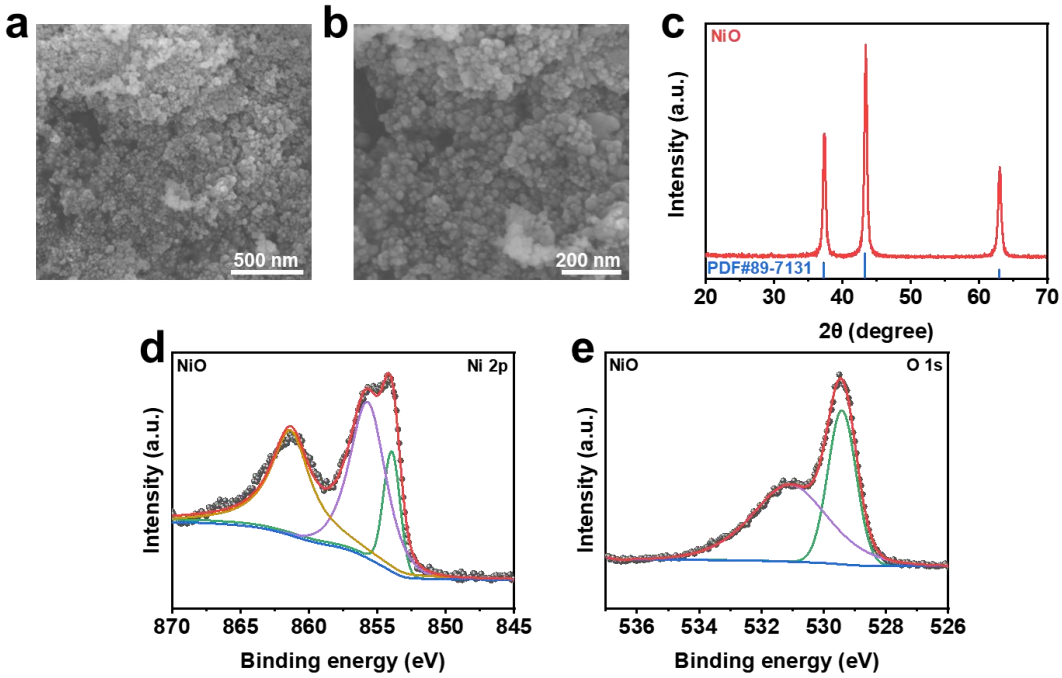

Figure S26. (a)-(b) SEM images and (c) XRD pattern of NiO electrocatalyst. XPS spectra of NiO electrocatalyst in the regions of (d) Ni 2p and (e) O 1s.

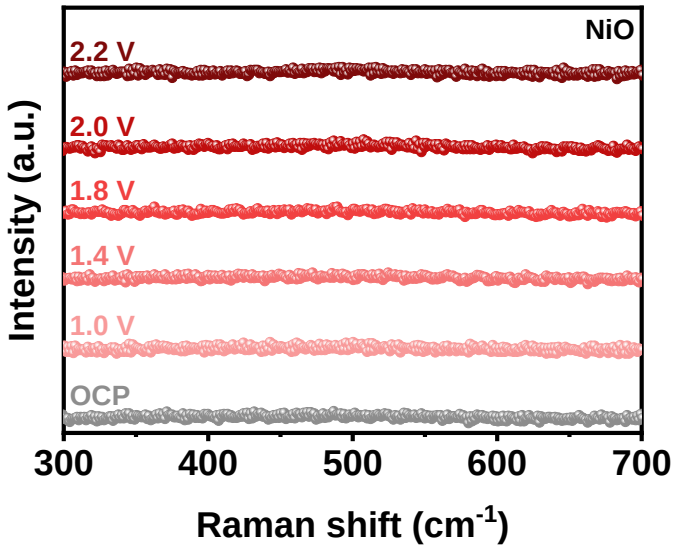

Figure S27. *In situ* electrochemical Raman spectra of NiO during N_2H_4 synthesis.

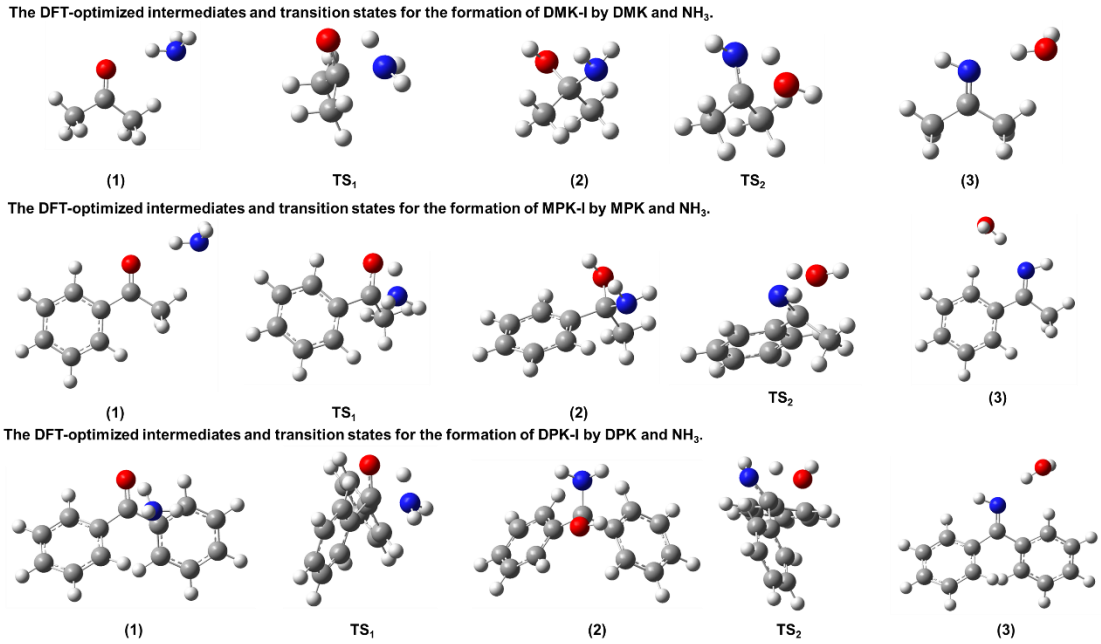

Figure S28. The DFT-optimized intermediates and transition states for the formation of different imines by ketones (DMK, MPK, and DPK) and NH_3.

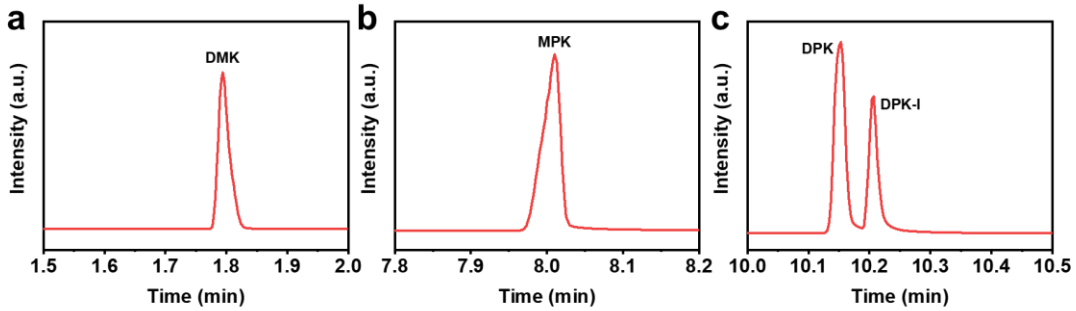

Figure S29. GC-MS analysis of imine formation from (a) DMK, (b) MPK, and (c) DPK ketones. Each ketone was mixed with NH_3 in CH_2Cl_2 and allowed to react overnight.

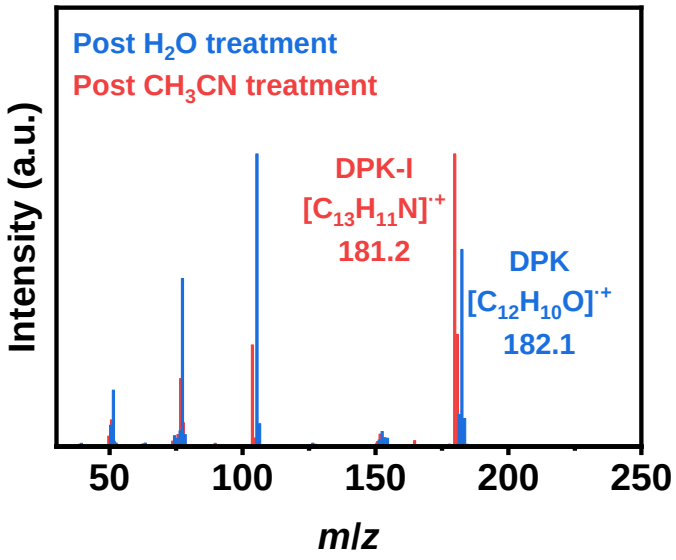

Figure S30. GC-MS spectra of DPK and DPK-I products after treating DPK-I in H_2O and CH_3CN solvents.

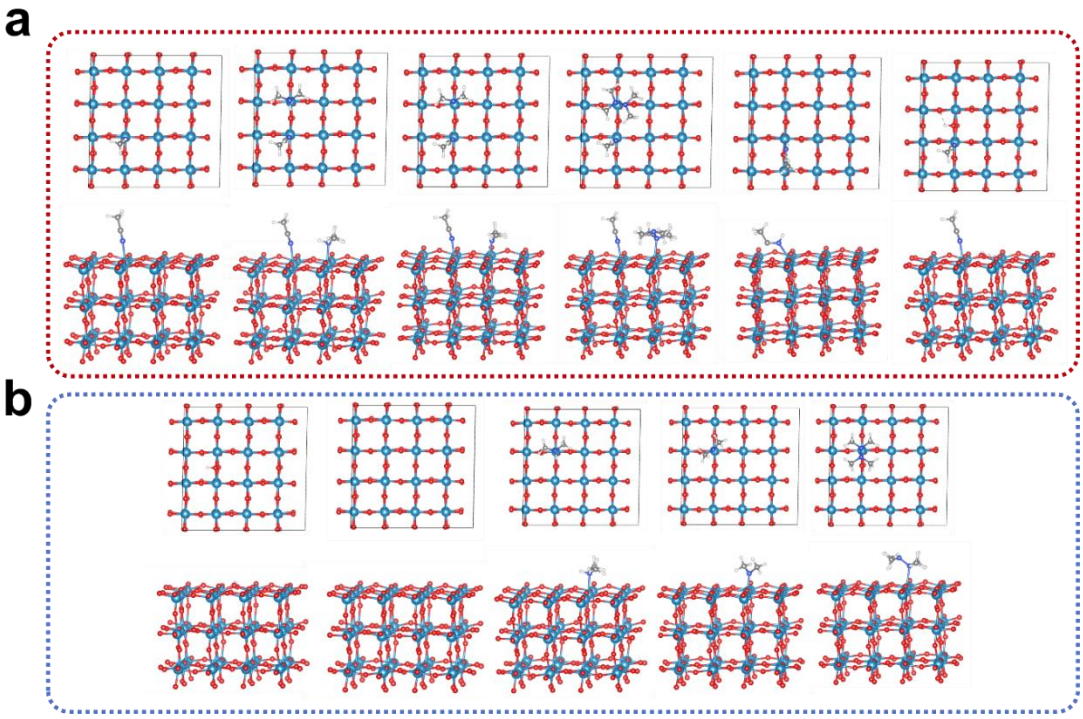

Figure S31. Atomic configurations of the intermediates on WO_3 (200) model (a) with and (b) without CH_3CN.